Distribution of Proton-Induced Transients in Silicon Focal Plane Arrays

Christina L. Howe, *Student Member, IEEE*, Robert A. Weller, *Senior Member, IEEE*, Robert A. Reed, *Member, IEEE*, Brian D. Sierawski, *Member, IEEE*, Paul W. Marshall, *Member, IEEE*, Cheryl J. Marshall, Marcus H. Mendenhall, Ronald D. Schrimpf, *Fellow, IEEE*, and John E. Hubbs, *Member, IEEE*

***Abstract*—Proton-induced energy deposition in a silicon P-i-N focal plane array is analyzed with Monte Carlo based simulations. These simulations include all physical processes, including events resulting from multiple particles incident on a single pixel, to describe the experimental data accurately. Post-processing of Monte Carlo simulations is done to account for the effects of pile up (multiple hits on a single pixel during one integration time) and non-radiation-induced noise in experiment. The results are compared with experimental data, and demonstrate how direct ionization dominates the cross section, yet fluctuations in *dE/dx* cause a broad range of energy depositions not addressed by an average LET calculation. An event rate is predicted for a full space proton flux and the dominance of direct ionization is shown and compared to computation using constant LET methods in CREME96. This comparison shows that at lower energies, CREME96 sufficiently predicts the event rate, but at higher energies a high fidelity simulation method is needed to capture the distribution.**

***Index Terms*—Energy deposited, event rate, focal plane array, Geant4, Monte Carlo, pile up.**

I. Introduction

HYBRID focal plane arrays (FPA) are used in space applications because of their flexibility in infrared applications, reliability, low cost, high resolution, and on-chip signal processing [1]. FPAs have important applications for satellite missions such as space-borne astronomy, Earth surveillance, star tracking, digital imaging, laser communications, etc. They are often used on satellites planned for long duration orbits in harsh proton environments requiring exceptional reliability when exposed to radiation. Because of their high sensitivity to noise, FPAs present a unique challenge in radiation hardness. Optical currents are small and near noise levels, so a single particle can produce enough charge to disrupt a signal [2]. Fig. 1 shows how the image produced by an optical sensor can be degraded by a solar proton event [3]. The image on the left in Fig. 1 captures a coronal mass ejection occurring on August 26, 2001. Coronal mass ejections are very rich in protons, increase the solar wind velocity, and can reach satellites in Earth's orbit quickly. The image on the right shows the image produced by a charge-coupled device (CCD) over an hour later degraded due to transient proton events. Spacecraft shielding helps mitigate incident electrons, but does not protect against protons, which also deposit energy and create secondary electrons. Hybrid visible array technology is especially important due to advantages over CCD-based imagers in high proton exposure applications. CCDs require collected charge to be transferred many times before being readout, and a loss of charge through proton induced traps can occur [4]. Hybrid FPAs require at most one transfer, thereby reducing the trapping vulnerability. On the other hand, a silicon P-i-N device can have quite a thick collection volume, which makes the quantitative evaluation of the sensitivity to proton-induced transients an important issue.

A better understanding of how radiation deposits energy in these devices will help lead to better prediction techniques and a greater understanding of experimental results. Accurate modeling tools will help designers predict the on-orbit response of these devices. In this paper we demonstrate a high-fidelity rate-prediction approach, based on Monte Carlo simulation and a mathematical model that accounts for multiple events that affect a single pixel during the integration time. Previous work has shown the ionization spectrum for a detector is different from the energy loss spectrum of particles causing the ionization [5]. In [6], it is noted that a constant LET approximation is a good assumption for some applications, but not all. In this paper we will quantify through simulation and experiment how using a single-value LET and path length calculation does not capture the full distribution.

II. Experimental Description

Hybrid focal plane arrays consist of a readout integrated circuit (ROIC) and detector array fabricated separately and then joined together with interconnects such as indium columns [2]. Fig. 2 shows the structure of a generic hybrid FPA [7]. The focal plane arrays in this study are well characterized visible-light, back-side illuminated FPAs consisting of a silicon P-i-N

Manuscript received July 17, 2007; revised September 3, 2007. This work was supported in part by NASA Electronic Parts and Packaging (NEPP) program and the Defense Thread Reduction Agency (DTRA) Radiation Hardened Microelectronics Program under IACRO #07-4201i to NASA, as well as the Medical Free-Electron Laser (MFEL) Program. The computational portion of this work was conducted through Vanderbilt University's Advanced Computing Center for Research and Education (ACCRE).

C. L. Howe is with the Department of Electrical Engineering and Computer Science, Vanderbilt University, Nashville, TN 37235 USA (e-mail: christina.l.howe@vanderbilt.edu).

R. A. Weller, R. A. Reed, and R. D. Schrimpf are with the Department of Electrical Engineering and Computer Science and the Institute for Space and Defense Electronics, Vanderbilt University, Nashville, TN 37235 USA.

B. D. Sierawski is with the Institute for Space and Defense Electronics, Vanderbilt University, Nashville, TN 37235 USA.

P. W. Marshall is a consultant in Brookneal, VA 24528 USA.

C. J. Marshall is with NASA/GSFC, Greenbelt, MD 20771 USA.

M. H. Mendenhall is with the Vanderbilt University Free Electron Laser Center, Nashville, TN 37235 USA.

J. E. Hubbs is with Ball Aerospace and Technologies Corporation, Albuquerque, NM 87117 USA.

Digital Object Identifier 10.1109/TNS.2007.909511

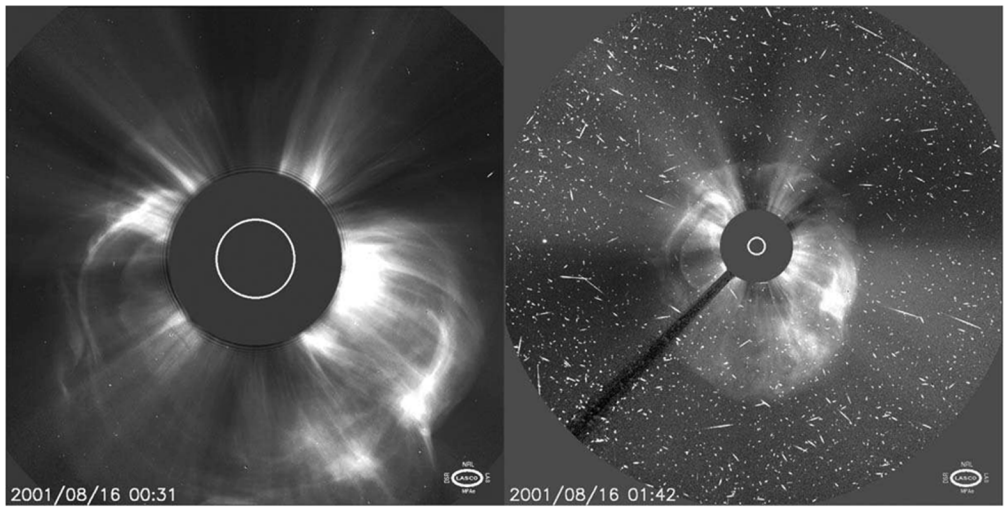

Fig. 1. Coronal mass ejection captured by LASCO on August 26, 2001. Over an hour later, degradation of the image produced by the optical detector can be seen on the right figure [3].

128×128 detector array with a radiation hardened complementary metal–oxide semiconductor (CMOS) ROIC and pixel pitch of 60 μm [8]. Proton radiation studies were performed at the Crocker Nuclear Laboratory (CNL) of the University of California, Davis (UC Davis). Full radiometric characterizations were performed at each radiation dose level to determine the impact of the radiation on dark current, noise, responsivity, sensitivity, and dynamic range both pre and post radiation [8]. In [8], we describe the total-ionizing-dose response of this array. This paper focuses on the proton-transient data, acquired at low fluxes, generating sparse hits to the array with 63 MeV protons at an angle of 45 degrees. The detectors were biased at 15 V, resulting in full depletion. Exposures were carried out at 233 K with temperature monitored by two radiation-hardened sensors not in the proton beam. Protons were incident on the silicon detector and then passed through the ROIC.

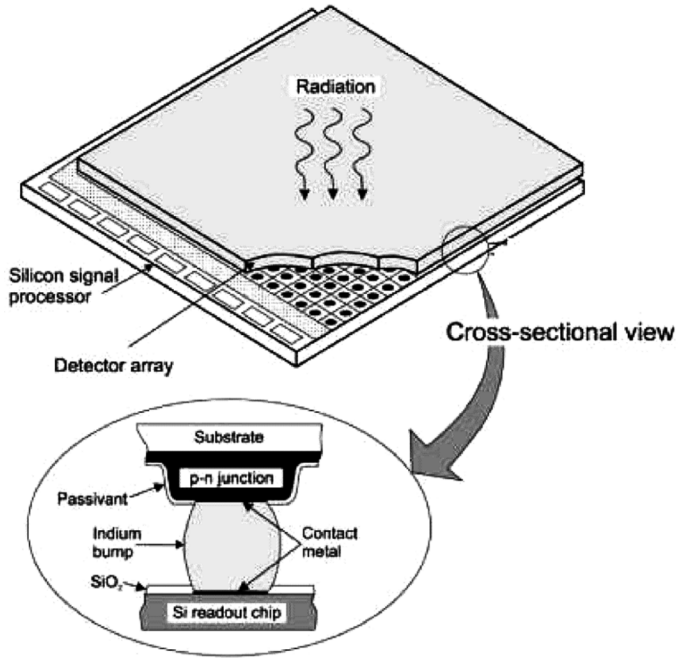

Fig. 2. Generic hybrid FPA with indium bump bonds [7].

III. Modeling Focal Plane Detectors

A. Monte Carlo Simulations

The radiation-transport Monte Carlo code used in this study is MRED (Monte Carlo Radiative Energy Deposition), a Geant4 based tool [9], [10], [11]. The structure used to simulate the focal plane detectors is shown in Fig. 3. The sensitive region corresponds to the region in which energy deposition must occur to produce a transient event. The top and bottom of the sensitive volume are flush with the top and bottom of the surrounding material, which is also silicon.

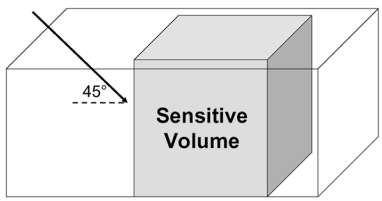

Fig. 3. Structure used to represent one pixel of a silicon p-i-n detector array. The entire structure is made of silicon and the shaded region is sensitive to the proton irradiation.

Simulations using MRED included physics processes that are relevant for radiation effects applications, including electromagnetic and hadronic processes, and elementary particles that live long enough to be tracked [11]. The effects of the finite integration time were simulated in a manner analogous to the computation of pile up in an ordinary nuclear spectrum. Each event in the Monte Carlo simulation represents one, and only one, primary particle. For finite integration times, there is a small but non-negligible probability of multiple hits on a single pixel (pile up). Two non-adjustable parameters are used in post processing the MRED simulations. The first is μ, the mean number

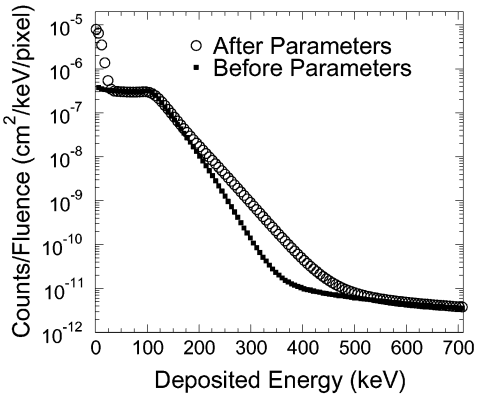

Fig. 4. MRED simulations before and after the effects of pile up and non-radiation-induced noise are applied.

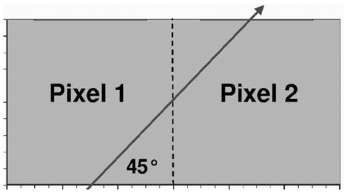

Fig. 5. TCAD structure representing two pixels. Simulations include detailed device parameters.

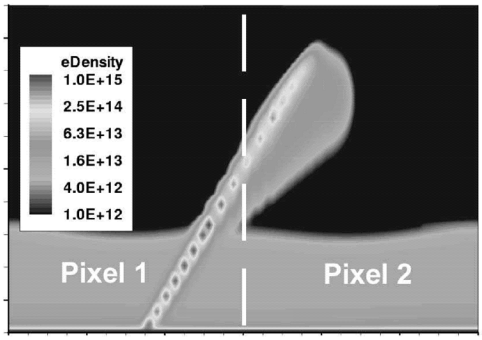

(a)

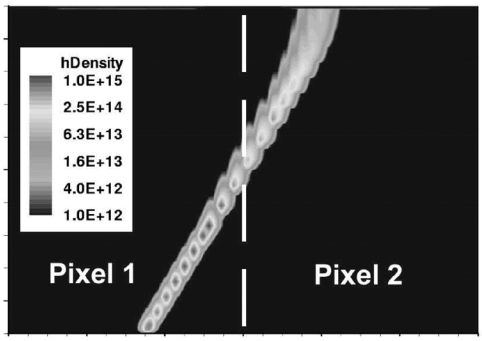

(b)

Fig. 6. (a) Electron density and (b) hole density 90 ps after a strike that spans two pixels equally. The motion of charged particles is not only vertical, but along the strike as well.

of proton hits per pixel during a single integration time, and is computed by

$$\mu = \sigma_{\rm sim}\phi\tau_{\rm int} \tag{1}$$

where $\sigma_{\rm sim}$ is the integral cross section of the simulation, ϕ is the experimental flux, and $\tau_{\rm int}$ is the experimental integration time. The second parameter is the addition of the non-radiation-induced noise observed in the experimental data. There is an approximately Gaussian broadening of pixels in the zero energy deposition range that represents the amount of system noise present. We applied a Gaussian convolution to the simulation and noise curves to fold the system noise into the simulation.

Fig. 4 compares the differential spectrum of MRED simulations before and after the effects of pile up and the non-radiation-induced noise were included in post-processing of the data. The shape of the sloped region between 125 and 500 keV is affected by the finite number of pixels that receive multiple hits during one integration period. The correction applied is a very general transformation of an arbitrary single-particle spectrum for the case in which the average number of hits per pixel is μ and similar to that described in [12]. The transformation inherently includes multiple hits of all orders, and can be used without numerical difficulty from very low fluxes well into the photon-counting region, where tens or hundreds of particles can hit a pixel in a single integration period. The region of very low energy is affected by the addition of the observed system noise.

B. TCAD Simulations

Technology computer aided design (TCAD) simulations were conducted based on an assumption of pixel structure. Fig. 5 shows the TCAD structure used to represent two adjacent pixels. Charge transport and collection within the device was simulated for various strike locations from a 63 MeV proton incident at 45 degrees. For each strike location, approximately 10% less charge was collected on the pixel taking the initial strike, and 10% more charge than expected was collected on the other pixel. The expected collected charge was calculated using a rectangular parallelepiped (RPP) approximation of pathlength and LET.

The motion of electrons and holes can be seen in Fig. 6. Note how the electrons and holes move not only vertically, but along the charge strike as well. This shows that the strike can become a temporary conducting path, causing more charge to collect on the second pixel, as noted above. If the pixels were completely isolated from one another, charge would move only vertically.

Fig. 7 shows the electric field and electrostatic potential 90 ps after a strike that spans two pixels equally. There is a slight disturbance in the electric field where the two pixels meet, but for the most part they stay relatively isolated. There is likewise a slight disturbance in the electrostatic potential, but it is minimal and will restore quickly to equilibrium. Since the effects of charge sharing between pixels is at maximum 10%, it suggests that the RPP assumption is sufficient to estimate the device response for this technology.

IV. Comparison With Experimental Data

In this section, we discuss simulations that mimic the experimental conditions: protons incident at an angle of 45 degrees

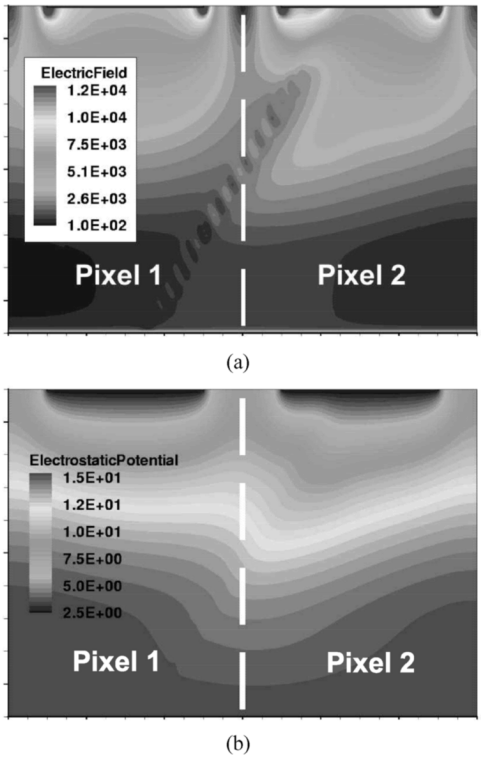

Fig. 7. (a) Electric field and (b) electrostatic potential 90 ps after a strike that spans two pixels equally. The electric field and electrostatic potential are only slightly perturbed suggesting that an RPP approximation for MRED simulations is sufficient for this technology.

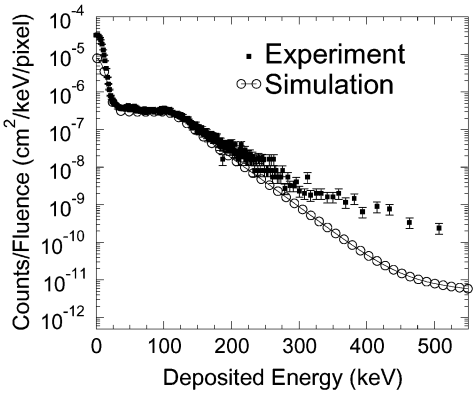

Fig. 8. Differential spectrum of counts per unit fluence per pixel for 63 MeV protons incident on the silicon detector structure from Fig. 3 compared with experimental results. The computed and measured total cross sections agree closely with each other and approximate the geometric cross section.

with energy of 63 MeV. The inclusion of all physical radiation transport processes in the simulation, accounting for pile up, and the inclusion of the measured random noise spectrum provide an accurate description of the experimental data for this device with no adjustable parameters. Fig. 8 shows a differential spectrum of the counts per fluence per pixel as a function of the energy deposited in the sensitive volume, comparing the simulation results with the experimental data. The conversion gain of the experimental data was extracted from the device parameters

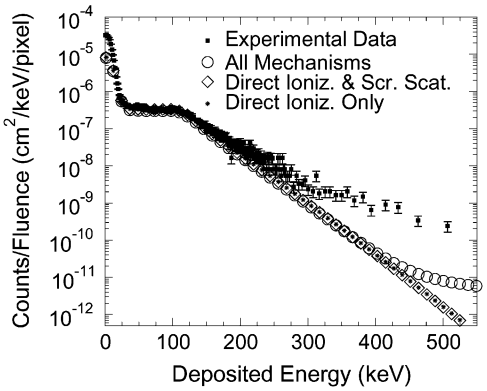

Fig. 9. MRED simulations comparing reaction mechanisms with experimental results. The large open circles represent the simulation of all physics processes available, the open diamonds include direct ionization and screened Rutherford (Coulomb) scattering, and the small stars include only direct ionization. Direct ionization is the dominant mechanism at lower energies, while nuclear reactions dominate at higher energies and screened scattering contributes little as expected.

characterized during device testing. The agreement between the two curves is excellent between 0 and 300 keV.

At higher energies, a few factors are possibly contributing to the difference between the two curves. First, there is an identified issue with the nuclear reaction models used by Geant4 [13]. This systematic error makes it difficult to simulate the sensitive region where nuclear reactions begin to dominate. Another contributing factor is oversimplification of the structure. Secondary particles produced by interactions with materials underneath the pixels may be recoiling back towards the array. These recoils can be lower in energy and highly ionizing. Simulations including the entire pixel array and underlying materials will reveal if these recoils are responsible for the uncertainity in the tail region. All possibilities are actively being researched further.

In Fig. 9, we compare MRED simulations for three situations: inclusion of all physics processes available in the simulation [11], direct ionization and screened Rutherford (Coulomb) scattering only, and direct ionization only with experimental results. At energies below 450 keV, direct ionization dominates the device response. Screened scattering contributes little to the cross section for this structure, as expected for 63 MeV protons since the nuclear stopping power is 2500 times smaller than the electronic stopping power at this energy.

The dashed lines in Fig. 10 represent the expected average and maximum energy deposited in the structure from a constant-LET and path length distribution calculation. The dashed line labeled “Avg” is the energy deposited along an average path length through one pixel, and the dashed line labeled “Max” is the energy deposited along a maximum path length. The maximum amount of energy deposited in the structure via this calculation is approximately 130 keV. Based on a constant LET analysis, no events are considered that deposit energy greater than this value. Therefore, a constant LET model does not describe the shape of the curve above 130 keV. The constant LET approximation considers only direct ionization, which is the dominant mechanism, but a path length analysis can only address averages while even primary ionization has fluctuations.

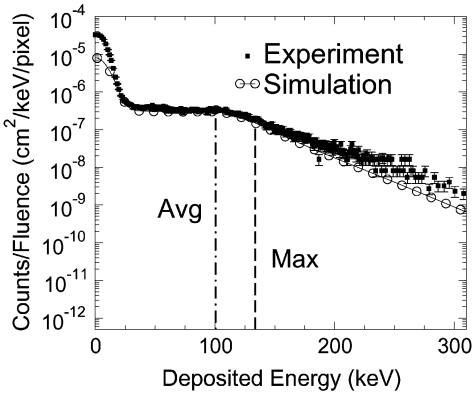

Fig. 10. Differential spectrum comparing the simulation results with experimental data and a constant LET path length calculation. The path length calculation does not predict the occurrence of large energy depositions.

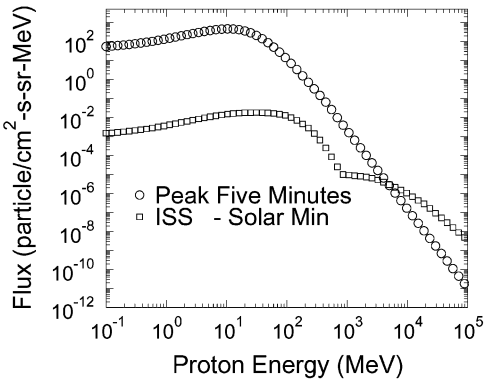

Fig. 11. Proton environments calculated using CREME96 [14]. The "GEO" curve is for the peak five minutes in geosynchronous orbit and "ISS" is for space station orbit using ap8min for solarmin.

V. Event Rate Predictions From Space Proton Fluxes

In this section, we consider the event rate for proton environments computed using MRED and compare these results to CREME96. For this calculation, simulations were done with an omnidirectional ion fluence. Fig. 11 shows the environment models used in the calculations in this section. The curves were computed using CREME96 [14]. The curve labeled "GEO" is for the peak five minutes in geosynchronous orbit while the "ISS" curve represents the international space station orbit using ap8min [15] for solarmin.

Fig. 12 presents the integrated event rate in events per pixel per day as a function of deposited energy for the peak five minutes in the geosynchronous orbit proton environment. MRED simulations show that when the full proton spectrum is considered, direct ionization dominates at energies below 2.75 MeV (125 fC). Fig. 12 also presents event rate calculations done with CREME96, which only consider direct ionization. At energies below 1.75 MeV (80 fC), there is good agreement between the MRED simulations and the CREME96 results. However, if the default value for the minimum energy in the LET spectrum of 0.1 MeV/nuc is used in the CREME96 calculation, the event rate is overestimated by as much as four orders of magnitude at higher energies. This overestimation is due to the limited range of protons in large silicon volumes, which is not considered by

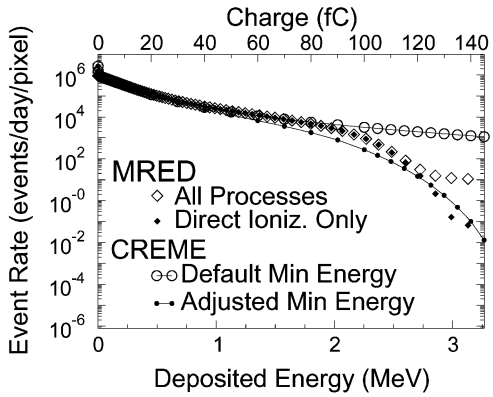

Fig. 12. Simulation results of the expected event rate from geosynchronous peak five minute proton environment in Fig. 11 through the pixel structure. Direct ionization dominates below 2.75 MeV (125f C). To accurately predict the event rate at higher energies using CREME96, the minimum energy in the LET spectrum must be properly adjusted.

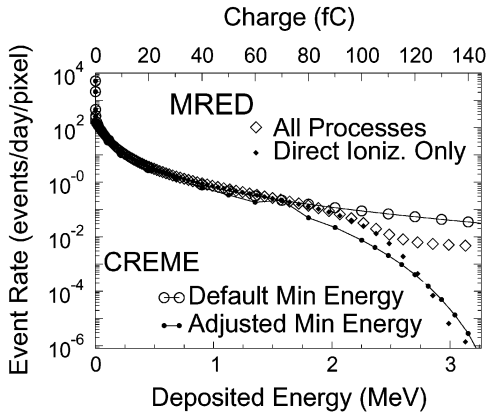

Fig. 13. Simulation results of the expected event rate from ISS orbit solar min proton environment in Fig. 11 through the pixel structure. As expected, the event rate is several orders of magnitude lower than the expected geosynchronous rates, but once again, incorrect adjustment of the CREME96 parameters could result in an over prediction of event rate.

the CREME calculation. This is noted on CREME96's website and its authors suggest this parameter be adjusted for certain SEU applications [14]. When a minimum energy value of 1.25 MeV/nuc is used in the CREME96 calculation, the event rate is comparable to the event rate obtained through MRED simulations. This value was obtained by fitting to the MRED simulations. So for applications in the low energy regime, such as those used for ground testing, CREME96 is a good predictor of device response. However, at higher energies expected in space, a high fidelity simulation is needed to avoid overestimating the event rate by not properly adjusting the minimum energy at which ions should be tracked.

When the same calculation is done for the international space station orbit, again we find that below 2.5 MeV, the rate is dominated by direct ionization, as in Fig. 13. As expected, due to lower proton fluxes, the event rate is several orders of magnitude lower than the geosynchronous rate. The default CREME96 parameters again overestimate the event cross section by several orders of magnitude unless the minimum energy parameter is adjusted to 1.25 MeV/nuc. A high fidelity simulation done with MRED predicts the event rate intrinsically.

VI. Conclusion

We have shown the effects of individual mechanisms on spectral shape that can be separated and studied individually. Through Monte Carlo based simulation, we show that direct ionization is the dominant mechanism for energy deposition below 300 keV in the focal plane detector considered here, while nuclear reactions dominate at higher energies and screened Rutherford scattering contributes very little. Even though direct ionization is the dominant mechanism, a constant LET and path length calculation does not address the fluctuations in *dE/dx*, only the variation in path length, and therefore does not capture the shape of the differential distribution. The methodology used in this paper can be extended to predict the implications of a full space proton flux. A high fidelity simulation is needed to accurately predict the device response at higher energies.

References

[1] D. A. Scribner, M. R. Kruer, and J. M. Killiany, "Infrared focal plane array technology," *Proc. IEEE*, vol. 79, no. 1, pp. 66–85, Jan. 1991.

[2] J. Pickel, "Novel devices and sensors," presented at the 1993 IEEE Nuclear and Space Radiation Effects Conf. Short Course, Snowbird, UT, Jul. 1993.

[3] Solar and helispheric observatory website. 2007 [Online]. Available: http://sohowww.nascom.nasa.gov

[4] P. W. Marshall and C. J. Marshall, "Proton effects and test issues for satellite designers," presented at the 1999 IEEE Nuclear and Space Radiation Effects Conf. Short Course, Norfolk, VA, Jul. 1999.

[5] H. Bichsel, "Energy loss and ionization of fast charged particles in a 20μm silicon detector," *Nucl. Instrum. Methods Phys. Res. A*, vol. 235, pp. 174–179, 1985.

[6] T. E. Button, W. F. Woodward, and T. S. Lomheim, "Simulation of proton-induced transients on visible and infrared focal plane arrays in a space environment," *Proc. SPIE*, vol. 3063, pp. 77–101, 1997.

[7] A. Rogalski, "HgCdTe infrared detector material: history, status, and outlook," *Rep. Prog. Phys.*, vol. 68, pp. 2267–2336, 2005.

[8] J. E. Hubbs, M. E. Gramer, D. C. Arrington, G. A. Dole, D. Maestas-Jepson, and S. E. Takeall, "Total ionizing dose and proton radiation characterization of Si p-i-n visible hybrid focal plane arrays," *Proc. SPIE*, vol. 5902, pp. 128–142, 2005.

[9] C. L. Howe, R. A. Weller, R. A. Reed, M. H. Mendenhall, R. D. Schrimpf, K. M. Warren, D. R. Ball, L. W. Massengill, K. A. LaBel, J. W. Howard Jr., and N. F. Haddad, "Role of heavy-ion nuclear reactions in determining on-orbit single event error rates," *IEEE Trans. Nucl. Sci.*, vol. 52, no. 6, pp. 2182–2188, Dec. 2005.

[10] S. Agostinelli *et al.*, "Geant4—A simulation toolkit," *Nucl. Instrum. Methods Phys. Res. A*, vol. 506, pp. 250–303, 2003.

[11] M. H. Mendenhall and R. A. Weller, "An algorithm for computing screened Coulomb scattering in Geant4," *Nucl. Instrum. Methods Phys. Res. B*, vol. 227, pp. 420–430, 2005.

[12] F. H. Tenney, "Ideal pulse pileup effects on energy spectra," *Nucl. Instrum. Methods Phys. Res. A*, vol. 219, pp. 165–172, 1984.

[13] R. A. Reed, R. A. Weller, M. H. Mendenhall, J. M. Lauenstein, K. M. Warren, J. A. Pellish, R. D. Schrimpf, B. Sierawski, L. W. Massengill, P. Dodd, N. F. Haddad, R. K. Lawrence, J. H. Bowman, and R. Conde, "Impact of ion energy and species on single event effects analysis," *IEEE Trans. Nucl. Sci.*, vol. 54, no. 6, pp. 2312–2321, Dec. 2007.

[14] Cosmic ray effects on micro electronics website. [Online]. Available: https://creme96.nrl.navy.mil/

[15] S. F. Fung, *Recent Development in the NASA Trapped Radiation Models*. New York: AGU Geophysical Monograph, 1996, vol. 97.